Kinetic Model of Ammonia Synthesis on Ruthenium via Programmable Surface Charge Modulation

Rajat Daga[1,2], Ulrick R. Gaillard[1,2], Jesse R. Canavan[1,2], Paul J. Dauenhauer[1,2], Matthew Neurock[1,2]*

[1] Center for Programmable Energy Catalysis, University of Minnesota, 421 Washington Ave. SE, Minneapolis, Minnesota, 55455, USA
[2] Department of Chemical Engineering & Materials Science, University of Minnesota, 421 Washington Ave. SE, Minneapolis, Minnesota, 55455, USA
*Corresponding author: mneurock@umn.edu

Abstract. Ammonia synthesis is kinetically constrained by the difficulty of dinitrogen activation and strong intermediate binding on transition metals. Recent advances in programmable catalysis have introduced the prospect of modulating the electronic properties of the catalyst in time, which can potentially circumvent the intrinsic catalytic kinetic limitations. Herein, we employ a multi-scale approach that integrates and expands the results from *ab initio* periodic density functional theory into kinetic monte carlo simulations to investigate the influence of static and programmable (i.e., dynamically oscillating) surface charge on the kinetics of ammonia synthesis over a model Ru surface. The computed turnover frequency exhibits a volcano-like dependence on surface charge, with a maximum at +0.05 $|e^-|$/Ru atom corresponding to a balance between the N_2 activation and NH_3 desorption. Dynamic surface charge oscillation across this optimum yields rate enhancements 20 times over the neutral surface and 10 times beyond the static volcano curve over different metals.

Introduction. Ammonia is critical to agricultural, chemical, and pharmaceutical processes, but it has also emerged as a promising medium for energy storage due to its high volumetric energy density and ease of storage and transportation. [1] To efficiently harness local energy sources, small-scale ammonia synthesis plants can be more optimal than large-scale facilities. [2] However, implementing small-scale NH_3 synthesis using the conventional Haber-Bosch process is inhibited by the need to activate strong N≡N bond that necessitates high operating temperature and pressure, thereby imposing significant energetic and infrastructural (i.e., capital) constraints. [3] Therefore, it is necessary to develop catalysts, catalytic paths, or processing conditions that can operate under moderate conditions while achieving higher single-pass conversion for the sustainable production of ammonia. [4]

Previous kinetic studies have explored the relationship between electronic properties of different transition metal catalysts and their efficacy in ammonia synthesis rate using the nitrogen atom binding energy as the primary descriptor of the rate. A volcano plot of the rate versus the nitrogen binding energy for pure metal catalysts suggests that Ru-based catalysts are closest to the Sabatier optimum. [5, 6] On metal catalysts like Fe, which exhibit stronger metal-nitrogen binding energies than those at the theoretical Sabatier peak, the surface tends to be saturated with NH_x* intermediates, leading to low H* surface coverage due to NH_3 re-adsorption followed by its dissociation and consequently decreased ammonia synthesis rate. [7, 8] Conversely, on metal catalysts like Ni with weaker metal-N binding energy than those at the theoretical Sabatier optimum peak, the surface coverages of NH_x* are significantly lower, which limits the formation and desorption of NH_3* species on the surface. [9] Recent advances have demonstrated that negatively charged Ru-based electrides can enhance ammonia synthesis rate by an order of magnitude, suggesting the strong influence of electronic properties of catalysts and supports in governing activity. [10, 11]

Dynamic modulation of catalyst electronic states has previously been used to transiently alter metal-adsorbate interaction and drive reactions toward enhanced selectivity and rate. [12, 13] This modulation has been previously applied to electrochemical systems by periodically oscillating between different applied potentials, thereby oscillating the

overall thermodynamics and kinetics of the reaction. [13, 14, 15] For gas-solid heterogeneous catalytic systems, computational studies have shown that modifying surface charge densities can perturb the electronic states of active sites, thereby resulting in changes in the binding energies, heats of reaction, and the activation barriers. [16, 17, 18] Recent experimental efforts have reported the development of catalytic condensers, which enable facile changes to the charge induced into supported catalysts using an external bias. [19, 20, 21] These devices have demonstrated the capability to oscillate applied potentials between +6 V and -6 V across Pt nanocluster catalyst particles and a dielectric layer, producing oscillatory charge variations of approximately ±1% of an electron per Pt atom. Catalytic condensers have since achieved substantially higher charge densities of 10^{14} $|e^-|/cm^2$ [20]. Microkinetic modeling has shown that to significantly increase reaction rates, oscillation frequencies exceeding the static turnover frequency of the reaction are needed. [22] Catalytic condensers maintain their charge accumulation upon periodic oscillation up to 3000 Hz [20], highlighting the experimental feasibility of this approach. However, the parameter space for studying reaction kinetics with a catalytic condenser is largely due to features absent from traditional catalysis research, such as the magnitude of charge storage, oscillation frequency, and duty cycle. [23] To identify the optimal parameter space, the details of how programmable modulation of surface charge influences elementary step kinetics and overall catalytic performance in ammonia synthesis need to be further explored.

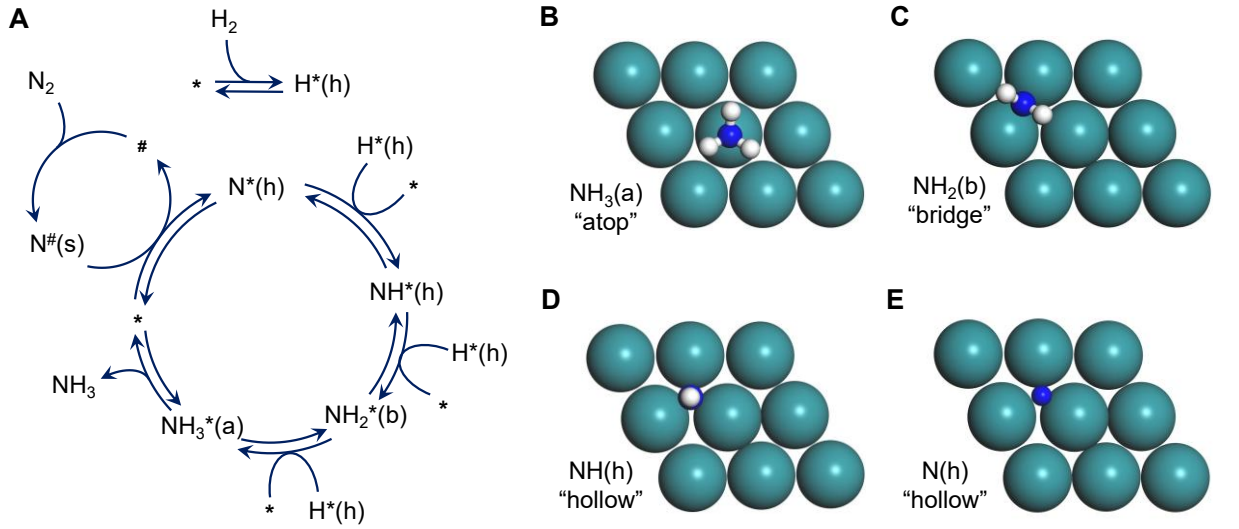

Figure 1. (A) The reaction mechanism for NH_3 synthesis on Ru surface on hollow, bridge, and atop sites (*) and step sites (#). The adsorbate configuration for **(B)** NH_3* on atop, **(C)** NH_2* on bridge, **(D)** NH* on hollow, and (E) N* on hollow site.

To quantify the influence of surface charge on reaction kinetics and identify non-equilibrium pathways, we developed a multi-scale kinetic modeling framework that combines the results from density functional theory (DFT) calculations together with molecular interaction models to establish the intrinsic elementary step kinetics as reactions proceed within kinetic Monte Carlo (kMC) simulations to examine ammonia synthesis over a stepped Ru(0001) surface subjected to surface charge densities between -0.17 $|e^-|$/Ru atom to +0.17 $|e^-|$/Ru atom. The mechanism for NH_3 synthesis on Ru is thought to proceed via dissociative adsorption of N_2 and H_2, followed by sequential addition of surface H* to the NH* intermediates that form, followed by desorption of ammonia, as presented in **Figure 1A**, with the most stable adsorption configuration for NH_x adsorbates shown in **Figure 1B-1E**. Our previous DFT results have determined the metal-adsorbate interaction and the kinetic parameters as a function of surface charge [Ulrick's paper]. This data is used in the kMC simulations along with DFT-parameterized molecular interaction models to determine the

elementary rate constants at each site at each time step to simulate the ammonia synthesis reaction network on Ru. It is shown that the peak turnover frequency (i.e., charge-modulated Sabatier peak) for static catalyst operation is attained at a surface charge of +0.05 $|e^-|$/Ru atom. By dynamically oscillating the surface charge across the optimum surface charge of +0.05 $|e^-|$/Ru atom, this multi-scale model predicts twenty-fold higher TOF than the neutral Ru surface. Furthermore, the optimal frequency to modulate the catalytic active site (*i.e.*, the resonance frequency) was identified as the maximum in the effective TOF.

To quantify the influence of surface charge on reaction kinetics and identify non-equilibrium pathways, we developed a multi-scale kinetic modeling framework that combines the results from density functional theory (DFT) calculations together with molecular interaction models to establish the intrinsic elementary step kinetics as reactions proceed within kinetic Monte Carlo (kMC) simulations to examine ammonia synthesis over a stepped Ru(0001) surface subjected to surface charge densities between -0.17 $|e^-|$/Ru atom to +0.17 $|e^-|$/Ru atom. The mechanism for NH_3 synthesis on Ru is thought to proceed via dissociative adsorption of N_2 and H_2, followed by sequential addition of surface H* to the NH* intermediates that form, followed by desorption of ammonia, as presented in **Figure 1A**, with the most stable adsorption configuration for NH_x adsorbates shown in **Figure 1B-1E**. Our previous DFT results have determined the metal-adsorbate interaction and the kinetic parameters as a function of surface charge [Ulrick's paper]. This data is used in the kMC simulations along with DFT-parameterized molecular interaction models to determine the elementary rate constants at each site at each time step to simulate the ammonia synthesis reaction network on Ru. It is shown that the peak turnover frequency (i.e., charge-modulated Sabatier peak) for static catalyst operation is attained at a surface charge of +0.05 $|e^-|$/Ru atom. By dynamically oscillating the surface charge across the optimum surface charge of +0.05 $|e^-|$/Ru atom, this multi-scale model predicts twenty-fold higher TOF than the neutral Ru surface. Furthermore, the optimal frequency to modulate the catalytic active site (*i.e.*, the resonance frequency) was identified as the maximum in the effective TOF.

Methods. *Density Function Theory Calculations.* The intrinsic elementary step energetics and kinetics used in the kinetic monte carlo simulations shown in **Figure 2** were parameterized using plane-wave periodic Density Functional Theory (DFT) as implemented within the Vienna Ab initio Simulation program (VASP). [24, 25, 26, 27] The Perdew−Burke−Ernzerhof (PBE) functional form of the generalized gradient approximation was used to calculate the energy corrections stemming from exchange and correlation effects. [28] Projector Augmented Wave (PAW) pseudopotentials were used to describe interactions between valence and core electrons. [29] The Ru(0001) surface was used as a model of the exposed hexagonally close-packed Ru surfaces. The Ru(0001) surface was constructed from the bulk hexagonal Ru crystal with lattice constants a = 8.1174 Å, b = 8.1174 Å, and c = 11.2608 Å and lattice angles of 90°, 90° and 120°. A 3 x 3 supercell of Ru(0001) was comprised of four Ru layers, with a surface coverage of 1/9 ML (i.e., one adsorbate per unit cell). In all of the calculations reported herein, the bottom two layers of the slab were held fixed while the top two layers were allowed to relax. A 20 Å vacuum was inserted to fully separate the Ru slabs. A 10x10x1 gamma-centered k-point mesh was used to sample the Brillouin zone (BZ). The DFT calculations utilized plane waves with an energy cutoff of 400 eV. An energy tolerance of 10^{-6} eV was used for self-consistent convergence. The geometries were converged to within a force cutoff of 0.02 eV/atom. *Kinetic Monte Carlo Simulations*. To simulate the kinetics of ammonia synthesis on the charged Ru surface, we carried out detailed kinetic Monte Carlo (kMC) simulations. An object-oriented C++ kinetic Monte Carlo (kMC) program developed by Hansen and Neurock [30, 31] was used to simulate dissociative adsorption of N_2 and H_2, hydrogenation and dehydrogenation of NH_x and desorption of NH_3 over a model Ru surface. To make the simulations initially tractable, we used the Ru(0001) surface as a simple first order model of the active Ru surface as it allows tracking of explicit surface site and lateral interactions. We utilized Unity Bond Index – Quasi Exponential Potential and DFT-calculated (UBI-QEP+DFT) kinetics on Ru(0001) surface but substituted the barrier of N_2 activation with the barrier calculated over the Ru B5 site, which is thought to be the active site. Details of the kinetic parameter calculation are elaborated in **Section 2** of

the supporting information. All of the explicit atop, bridge and hollow sites were considered within the kMC simulations. The kMC program utilized the intrinsic kinetics database established from the UBI-QEP+DFT-calculations to provide the base-level intrinsic kinetic parameters and proceeded via an iterative kMC algorithm which calculated the rates for all possible elementary kinetic steps including adsorption, reaction and diffusion, and assigned a probability of occurrence for each step. This was followed by the random selection of an elementary step that proceeded based on the kinetic probability and execution of the kinetic event on the surface. The kMC acceleration scheme developed by Dybeck–Neurock [32] was incorporated to rescale the fast equilibrated processes to increase the sampling of kinetically relevant steps. The iterative execution of kMC steps continued until an end criterion was met, followed by post-processing of the output data to calculate important output like the time evolution of the surface coverage of different intermediates and individual and overall reaction rates. The details of the algorithm are presented in **Section 1** of the supporting information.

To account for lateral interactions between surface adsorbates, the kMC program used molecular interaction models to determine the "Through Surface" and "Through Space" interactions between adsorbates on the surface. [31] "Through Surface" interactions involved the interactions between adsorbate species that share metal atoms. This sharing increased the metal atom coordination number, thus weakening all the bonds associated with that metal atom. The weakening of metal-adsorbate bonds was captured using UBI-QEP. [33, 34] "Through Space" interactions involved interactions between the electron cloud of neighboring atoms through space. These were accounted for using the van der Waal and electrostatic terms from the MMFF94 force field. [35] The interaction models were parameterized using DFT-calculated binding energies of NH_3*, NH_2*, NH*, N* and H* as a function of surface coverage. These parameterized interaction models were used to calculate the influence of the local surface coverage on the intrinsic activation barriers on-the-fly within the kMC simulations. Further details on the parameterization of adsorbate-adsorbate interaction and the calculation of activation barriers as a function of surface coverage are provided in **Section 1** and **Section 2** in the supporting information.

All kMC simulations were performed under isothermal, isobaric conditions at 650 K and a total pressure of 50 bar, using a reactant gas mixture with a stoichiometric H_2:N_2 ratio of 3:1. The catalyst surface was represented by a 12 × 12 Ru atom grid with periodic boundary conditions applied in the lateral directions. A differential reactor configuration was assumed, such that once desorbed, gas-phase NH_3 was irreversibly removed from the system. A cutoff distance of 5.2 Å was employed to define the neighborhood for lateral interactions between adsorbed species.

Results and Discussion. In previous work, we employed periodic DFT calculations to calculate the binding energies for N*, H*, NH*, NH_2*, and NH_3* as a function of surface charge (**Figure 2A)**. The results presented in **Figure 2A** show that the binding energies of NH_3*, NH_2*, and NH* progressively become stronger in moving from -0.17 $|e^-|$/Ru to +0.17 $|e^-|$/Ru. The binding energies become considerably stronger at positive potentials. This is due to the presence of both covalent as well as coulombic interactions. At high positive charges, the negative charge on the nitrogen is "sandwiched" between the strong positive charge plane of the metal and the strong positive charge plane of the hydrogen on NH_x (x = 1-3), thus creating a "charge sandwich" with strong coulombic interactions. This significant strengthening at high charges is strongest for NH_3* and systematically decreases for NH_2* and NH* due to the fewer protons, as shown in **Figure 2B**. The binding energies for N* and H* are relatively flat over the full range of charges.

The binding energies were used along with the gas phase energies to determine the energies for reaction as a function of charge, which are plotted in **Figure 2C**. The elementary step hydrogen addition reaction energies systematically become more favorable in moving from -0.17 $|e^-|$/Ru to +0.17 $|e^-|$/Ru. This is due to stronger increased binding energy curves in moving from N* to NH_3* due to enhanced coulombic stabilization. The N_2 reaction energy and the NH_3 desorption energy curves tend to be the limiting steps at more negative and positive charges, respectively. At more negative charges, N_2* is considerably stabilized due to electron transfer into the N_2 whereas it's product N* is considerably weaker at more negative charges

due to Pauli repulsion. As discussed above, the binding energy of NH_3* product is considerably weaker at negative charges and stronger at positive charges due to coulombic interactions. This leads to a systematic increase in the ammonia desorption reaction energy when going from negative to positive charge.

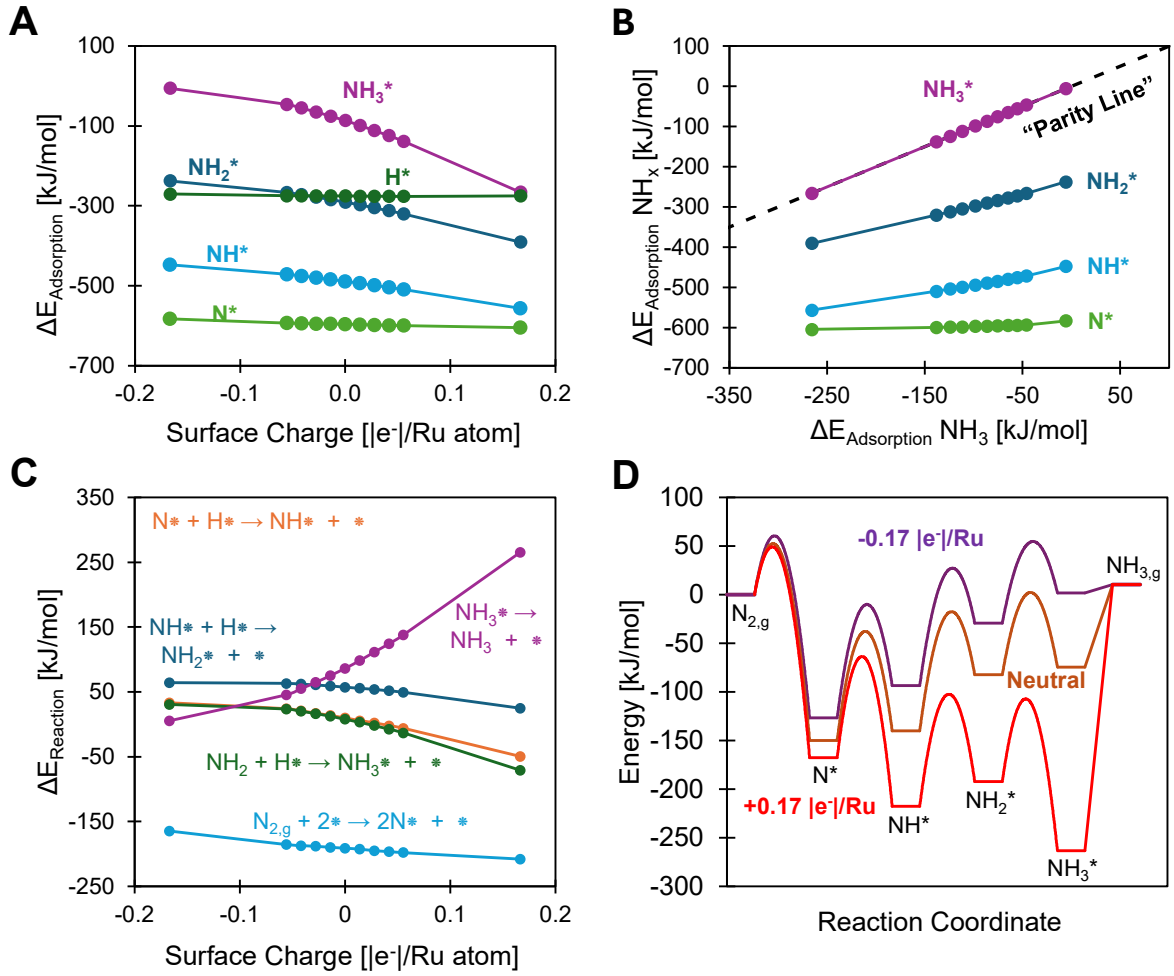

Figure 2. (A) DFT-calculated energy of adsorption for intermediate surface species as a function of surface charge. **(B)** DFT-calculated energy of adsorption for intermediate species relative to ammonia adsorption energy. **(C)** The DFT-calculated reaction energies for the N_2 activation, NH_x hydrogenation, and NH_3 desorption reactions as a function of surface charge. **(D)** The reaction coordinate diagram for -0.17 |e$^-$|/Ru atom, neutral, and +0.17 |e$^-$|/Ru atom surface charge.

The DFT-computed binding and reaction energies were used in conjunction with UBI-QEP theory [33, 36, 37] to estimate the low-surface coverage activation barrier for each elementary step as a function of surface charge, enabling charge-enhanced reaction coordinate energy diagrams to be made (**Figure 2D**). Further details on the estimation of barriers using UBI-QEP theory are provided in Section 2 of the supporting information.

The kinetic barriers derived from UBI-QEP+DFT theory for each elementary step on neutral Ru surface are summarized in **Table 1**. Although the activation barrier for N_2 dissociation on the Ru(0001) terrace is reported to exceed 200 kJ/mol [38], the present kinetic model employed the activation barrier of 40 kJ/mol corresponding to active B5 step-edge sites, comprising of five metal atoms with three metal atoms in the bottom edge and two metal atoms in the layer above the step edge. [8, 38, 39, 40] The concentration of B5 sites on Ru catalysts can range between 0.1%-30% of the number of surface atoms, depending on particle

morphology and size [41, 42]. To account for the limited availability of the active B5 sites, a 5% B5 site concentration was assumed in this work. Accordingly, the pre-exponential factor for N_2 activation, estimated using collision theory, is scaled by this factor to reflect the low concentration of step-edge sites on the surface. [43] The pre-exponential factors for surface-mediated steps were approximated as 10^{13} s^{-1} based on Transition State Theory (TST), while values for gas-phase dissociative adsorption for H_2 and N_2 were derived from collision theory (Section 2, supporting information). kMC simulations were then conducted using these parameters to estimate the turnover frequency (TOF), surface coverages, degree of rate control, and other relevant quantities under static and dynamic modulation of surface charges.

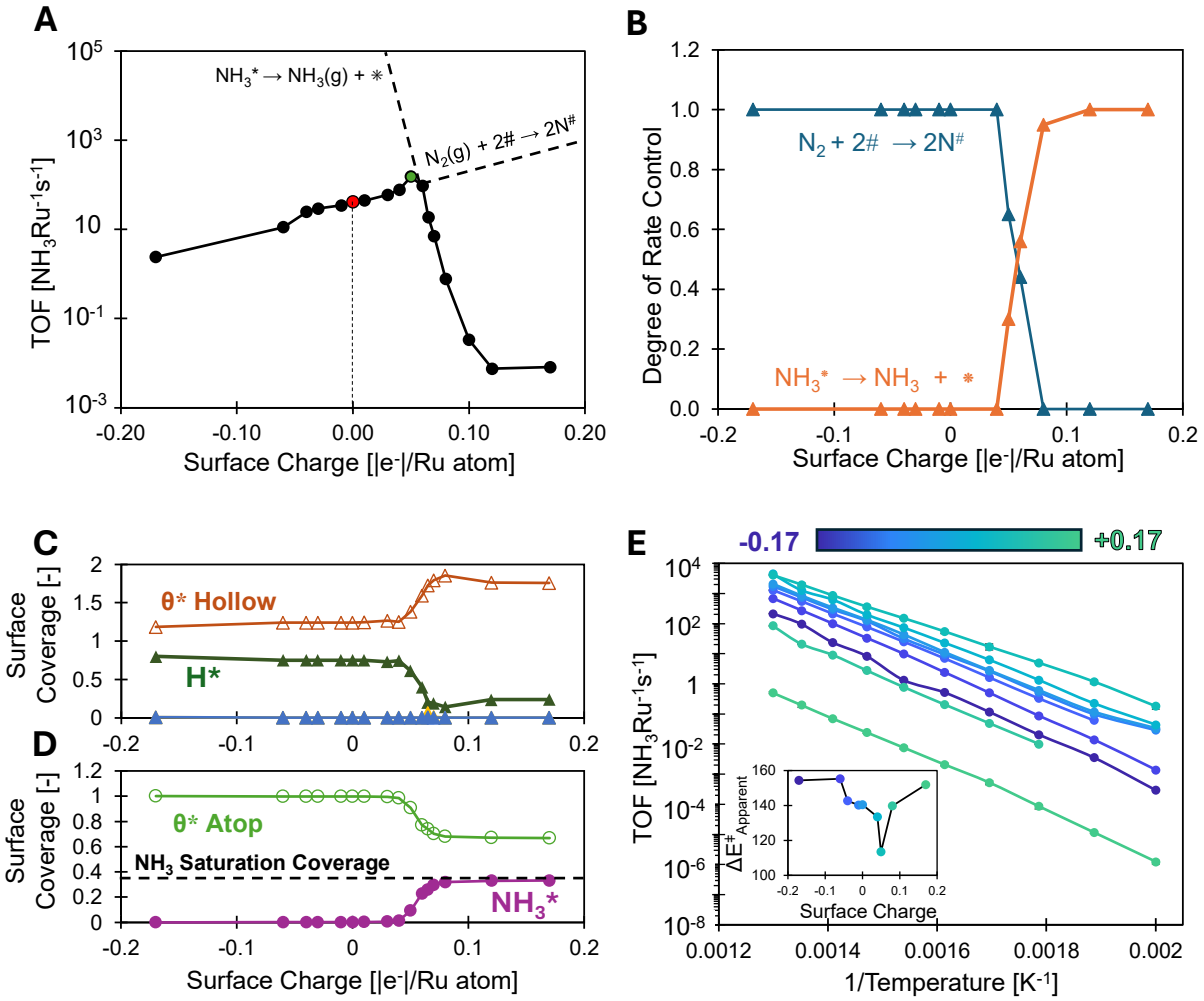

Figure 3. (A) The turnover frequency to form NH_3 simulated by kinetic Monte Carlo as a function of surface charge at 50 bar, and 650 K. The dashed lines represent the kinetics of the rate-determining steps at respective kinetic regimes on either side of the peak. **(B)** The degree of rate control for NH_3 synthesis and NH_3 desorption steps as a function of surface charge. **(C)** The surface coverage for reacting chemical species on hollow sites as a function of surface charge. **(D)** The surface coverage for species on atop sites as a function of surface charge. **(E)** Arrhenius plot for surface charges between -0.17 |e-|/Ru atom and +0.17 |e-|/Ru atom. Inset plot is the plot of apparent activation barrier as a function of surface charge.

The kMC simulations were first used to model the statically charged Ru surface and to construct a volcano curve for the reaction rates as a function of charge. Simulations were carried out for surface coverages from -0.17 |e-|/Ru to +0.17 |e-|/Ru and used to determine the turnover frequency (TOF) for

each charge. The results shown in **Figure 3A** indicate that there is a volcano-shaped dependence of the TOF on the charge with the optimal peak in TOF at +0.05 $|e^-|$/Ru atom. This optimum corresponded to a balanced Ru-N interaction strength, yielding the highest ammonia synthesis rate. This suggests that a stronger metal-N interaction is required to further enhance the yield of ammonia, in general agreement with the comparable observation on the metal Sabatier volcano plot. [5] Surface charges less than +0.05 $|e^-|$/Ru atom lead to a weaker Ru-N interaction and a higher N_2 activation barriers which resulted in a lower NH_3 synthesis rate. At surface charges greater than +0.05 $|e^-|$/Ru atom, while the barrier for N_2 activation decreases, the NH_3 desorption barrier increases, resulting in slower desorption of NH_3 from the surface. These changes are supported by the plot of degree of rate control (DRC) as a function of surface charge that is shown in **Figure 3B**. At charges <0.05 $|e^-|$/Ru atom, the DRC for N_2 activation = 1, whereas systems with charges that are > +0.06 $|e^-|$/Ru atom result in a DRC = 1 for NH_3 desorption. A crossover in DRC curve from N_2 activation to NH_3* desorption occurs at approximately +0.05 $|e^-|$/Ru atom, which corresponds to the peak of TOF plot at this charge.

Concurrently, the surface coverage plots of hollow and atop sites (*) in **Figure 3C** and **Figure 3D**, respectively, indicate a shift in the dominant surface species from H* at negative surface charges to NH_3* at highly positive surface charge, with NH_3* coverage saturating at 0.33 ML. Total hollow sites exhibit a coverage of 2ML since they comprise of hcp and fcc sites, each having 1 ML surface coverage. The NH_3* saturation coverage is consistent with previous experimental observations reporting sub-monolayer saturation of NH_3* on Ru(0001). [44] In addition, previous DFT calculations of NH_3* binding energy as a function of surface coverage suggested a maximum saturation surface coverage of 1/3 ML of NH_3* on the Ru(0001) surface [cite Ulrick].

kMC simulations were subsequently carried out as a function of temperature to construct the Arrhenius plot for different charges from -0.17 to +0.17 $|e^-|$/Ru, shown in **Figure 3E**. An apparent barrier of ~150 kJ/mol was calculated from the effect of thermal variations on rate at -0.17 $|e^-|$/Ru atom surface charge. To affirm the rate limiting steps derived from DRC, another method utilizing DRC and thermodynamic DRC (TDRC) of all elementary steps to estimate the apparent barrier were used as shown in the following equation, [45]

$$\Delta E^{\ddagger}_{App} = \sum_i X_{DRC,i}\Delta E^{\ddagger}_{Input,i} + \sum_i X_{TDRC,i}\Delta E_{Input,i}\,, \quad (1)$$

where $\Delta E^{\ddagger}_{App}$ is the apparent barrier, $X_{DRC,i}$ is the degree of rate control magnitude for i^{th} elementary step, $\Delta E^{\ddagger}_{Input,i}$ is the input barrier to kMC model, $X_{TDRC,i}$ is the thermodynamic degree of rate control magnitude for i^{th} elementary step, and $\Delta E_{Input,i}$ is the reaction energy.

The DRC and TDRC values were then used to derive the expression of rate constant for the kinetic regime as,

$$k_{app} = A \times \left(k_1 P_{N_2}\right)^{X_{DRC,1}} \times (k_6)^{X_{DRC,6}} \times \left(\frac{K_2}{P_{H_2}}\right)^{X_{TDRC,2}}, \quad (2)$$

where k_{app} is the apparent rate constant, A is a constant, k_1 is the rate constant for N_2 activation, P_{N_2} is the N_2 pressure in reactant gas mixture, $X_{DRC,1}$ is the degree of rate control of N_2 activation, k_6 is the rate constant for NH_3* desorption, $X_{DRC,6}$ is the degree of rate control of NH_3* desorption, K_2 is the equilibrium constant for H_2 dissociative adsorption and associative desorption, P_{H_2} is the hydrogen pressure in reactant has mixture, and $X_{TDRC,2}$ is the thermodynamic degree of rate control for hydrogen adsorption desorption equilibrium.

The dominant contributions to the apparent barrier at -0.17 $|e^-|$/Ru atom are from N_2 activation (50 kJ/mol; $X_{DRC,1}$ = 1; $X_{DRC,6}$ = 0) and hydrogen adsorption thermodynamic DRC (90 kJ/mol; $X_{TDRC,2}$ = 0.8). The sum of the two contributions resulted in an apparent barrier of 140 kJ/mol, close to the thermally calculated apparent barrier of 150 kJ/mol, suggesting that the rates are limited by N_2 activation and hydrogen poisoning. This is in agreement with previous experimental studies

which have shown that hydrogen blocks sites and reduces the rates of ammonia synthesis resulting in negative rate order of hydrogen ranging from -0.6 to -1.0. [46] The calculations for degree of rate control and thermodynamic degree rate control within the kMC framework are further described in the supporting information.

Increasing the charge in the kMC simulations from -0.17 to +0.05 $|e^-|$/Ru decreases the apparent barrier from 150 kJ/mol down to ~115 kJ/mol, as shown in the inset in **Figure 3E**. The contributions to the apparent barrier at +0.05 $|e^-|$/Ru atom comes from N_2 activation (24 kJ/mol; $X_{DRC,1}$ = 0.65), NH_3 desorption (46 kJ/mol; $X_{DRC,6}$ = 0.35), and hydrogen adsorption desorption equilibrium (36 kJ/mol; $X_{TDRC,2}$ = 0.3). Further increase in the positive surface charge increases the degree of rate control for NH_3* desorption ($X_{DRC,6}$) to ~1 and makes ammonia desorption the sole rate-controlling step. The strong binding at the positive charges that result from the coulombic attractive interactions discussed previously increase the apparent barrier for NH_3 desorption to ~150 kJ/mol. This apparent barrier is lower than the zero surface coverage NH_3 adsorption energy due to repulsive lateral interactions that occur at higher ammonia saturation surface coverage, resulting in weaker binding energy and therefore a lower barrier for ammonia desorption.

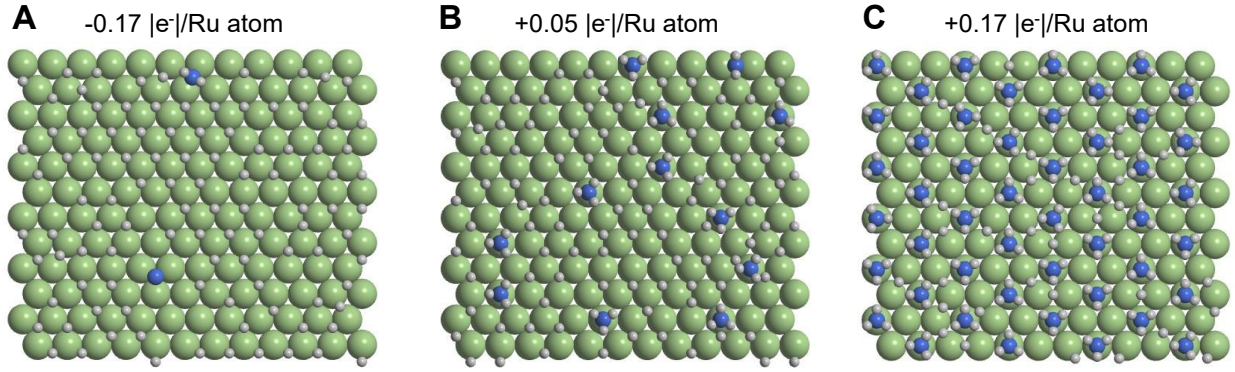

Figure 4. The surface from ammonia synthesis kinetic Monte Carlo simulations at 650 K and 50 bar at: **(A)** -0.17 $|e^-|$/Ru atom, **(B)** +0.05 $|e^-|$/Ru atom, and **(C)** +0.17 $|e^-|$/Ru atom. The green spheres are ruthenium atoms, the blue spheres are nitrogen atoms, and white spheres are hydrogen atoms.

The surface configurations and molecular arrangements of the simulated catalyst surface reported in **Figure 4** at different surface charges show a progression in the steady state surface composition. At negative surface charges, atomic surface hydrogen (H*) dominates the surface with few NH_x* species present on the surface such as that shown in **Figure 4A** for a surface charge of -0.17 $|e^-|$/Ru atom. This is due to weak Ru-N interaction at negative charge which results in a high activation barrier for N_2 activation, in agreement with previous studies reporting high surface coverage of H* on neutral Ru surface [47, 48]. The surface at +0.05 $|e^-|$/Ru atom shown in **Figure 4B** exhibits a more balanced distribution of H* and NH_x*, indicative of faster overall rates. Under these conditions, the hydrogenation reactions become increasingly more exothermic, and the rate-limiting step proceeds fast enough to disrupt the quasi-equilibration of the steps that are otherwise equilibrated under negative charges. At higher positive surface charge such as +0.17 $|e^-|$/Ru atom which is shown in **Figure 4C**, NH_3* binds very strongly to the surface reaching saturation surface coverages and blocking surface sites, thus inhibiting the rate.

The results from the detailed kMC simulation at different charges were subsequently used to explore programmable (i.e., forced dynamic) systems where the extent of surface charge condensation is oscillated. In order to do so, we first extracted the elementary rate constants for all the elementary steps as a function of charge from the simulations at different charges. More specifically, we then analyzed the changes that occur in modulating the potential from -0.17 to +0.05 $|e^-|$/Ru and from +0.05 to +0.17 $|e^-|$/Ru.

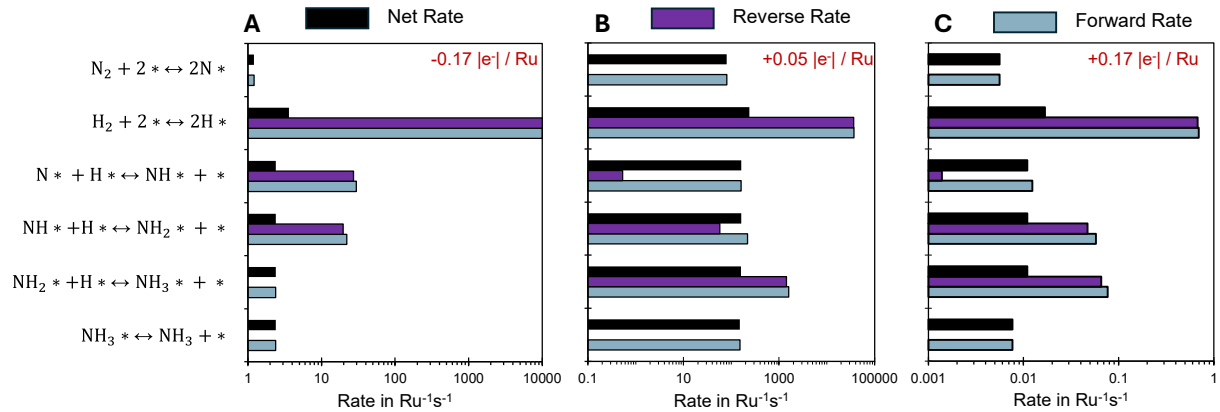

Figure 5. The rates of elementary steps for **(A)** -0.17 |e-|/Ru atom, **(B)** +0.05 |e-|/Ru atom and **(C)** +0.17 |e-|/Ru atom. The black bars represent net forward rate, purple bar represents reverse rate, and gray bar represents the forward rate. All reactions were simulated at 650 K and 50 bar.

Figure 5 depicts the reaction rates for the elementary steps at -0.17 |e-|/Ru atom, +0.05 |e-|/Ru atom, and +0.17 |e-|/Ru atom surface charges. The initial intrinsic barriers used for the above charges are listed in Error! Reference source not found.. For all surface charges, H_2 adsorption and desorption steps were e quilibrated and significantly faster than other steps. At -0.17 |e-|/Ru atom, N* hydrogenation and NH* hydrogenation steps are equilibrated as shown in **Figure 5A** due to lower barrier of NH* and NH_2* dehydrogenation steps than their hydrogenation steps. In moving from -0.17 |e-|/Ru to +0.17 |e-|/Ru, there is a change in the equilibrated reactions. At high positive charge of +0.17 |e-|/Ru atom, the NH* and NH_2* hydrogenation steps were equilibrated as shown in **Figure 5C** due to lower barrier for NH_2* dissociation and NH_3* dissociation than those for NH_2* hydrogenation and NH_3* desorption, respectively, resulting in higher NH_2* and NH_3* dissociation rates than NH_2* hydrogenation and NH_3* desorption. At the optimum charge of +0.05 |e-|/Ru atom, only the NH_2* hydrogenation step is equilibrated due to higher NH_3* desorption barrier than NH_3* dissociation barrier. While the NH* dissociation barrier is close to the NH* hydrogenation barrier, the high H* surface coverage promotes the NH* hydrogenation step. As a result, the NH* formation step is not equilibrated. Overall, the +0.05 |e-|/Ru atom system exhibits a weaker equilibrated regime as compared to other surface charges, enabling higher ammonia synthesis rates. The above presented shifts in surface coverage through surface charge modulation change the rate-determining steps and can potentially allow dynamic catalytic rate improvement by decoupling reaction steps [6].

The influence of forced dynamic charge modulation on catalytic conversion of N_2 and H_2 to NH_3 was evaluated by simulating square-wave oscillations between discrete surface charge states (*i.e.*, input charge programs). Three sets of charge oscillations have been evaluated, with a set of charges close to the optimum charge (+0.04 & +0.07 |e-|/Ru), charges farther away from the optimum charge of +0.05 |e-|/Ru atom (neutral & +0.14 |e-|/Ru atom), and the extreme charge case (-0.17 & +0.17 |e-|/Ru).

The first set of dynamic study involves oscillation between +0.04 and +0.07 |e-|/Ru which are close to the static optimum charge. kMC simulations employ a square wave oscillation function with 50% duty cycle (*i.e.*, equal time at each catalyst state). The corresponding reaction coordinate diagram for both the surface charges is shown in **Figure 6A**. An ideal catalytic turnover would proceed with N_2 activation and all the hydrogenation steps at +0.07 |e-|/Ru atom to form NH_3* on the surface followed by oscillation to +0.04 |e-|/Ru atom to enable faster NH_3* desorption. However, at +0.04 |e-|/Ru atom, the NH_3* dissociation barrier is lower than NH_3* desorption barrier resulting in preferential dissociation of NH_3* to NH_2*. This forms a 'leaky ratchet' system, wherein the intermediates are trapped in a catalytic loop rather than completing a catalytic turnover. [23, 49] This is illustrated in the temporal evolution of the surface coverage plot at 650 K and 10^3 Hz oscillation frequency in **Figure 8A** where NH_3* first accumulates on the surface at +0.07 |e-|/Ru and then desorbs from the surface at +0.04 |e-|/Ru at slower time scales than elementary step desorption rate primarily due to catalytic looping. This decreases the efficacy of charge oscillation, resulting in weak

dependence of TOF on the applied oscillation frequency, reflected through the lower slope of the TOF plot relative to the parity line in **Figure 6B**.

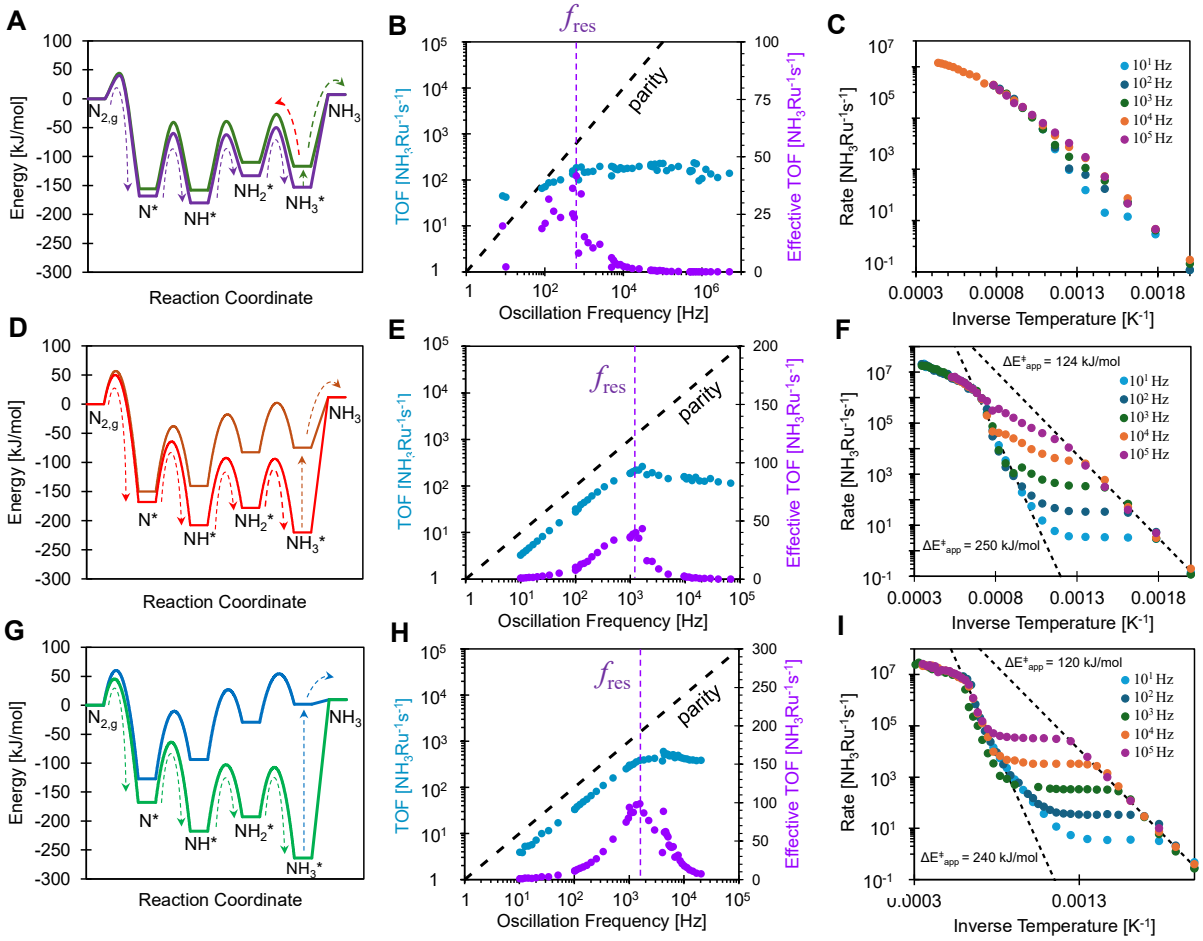

Figure 6. The reaction coordinate diagram for dynamic oscillation between: **(A)** +0.04 |e⁻|/Ru atom and +0.07 |e⁻|/Ru atom, **(D)** neutral and +0.14 |e⁻|/Ru atom, and **(G)** -0.17 |e⁻|/Ru atom and +0.17 |e⁻|/Ru atom. The dashed lines indicate the most favorable reaction path. The dashed red line in **(A)** indicates that NH_3 dissociation is favored over NH_3 desorption due to lower barrier. **(B, E, H)** The turnover frequency (TOF) and effective TOF as a function of applied oscillation frequency is shown in blue and purple data points, respectively, for the three considered oscillation amplitudes at 650 K and 50 bar total pressure. The black dotted line represents parity between applied frequency and catalytic TOF; the vertical purple dotted line identifies the resonance frequency. **(C, F, I)** Arrhenius plots for dynamic oscillation under varying oscillation frequencies of 10 Hz (light blue), 10^2 Hz (dark blue), 10^3 Hz (green), 10^4 Hz (orange) and 10^5 Hz (purple) for the three considered oscillation amplitudes at 50 bar total pressure.

The maximum TOF achieved under dynamic oscillation between this set of charges is 208 $NH_3Ru^{-1}s^{-1}$ at an applied catalyst oscillation frequency of 10^5 Hz, representing only marginal improvement over 190 $NH_3Ru^{-1}s^{-1}$ at 10^3 Hz. To account for the efficiency of catalytic ratchets and identify the resonance frequency, we use the turnover efficiency, η_{TOF}, effective TOF metric defined by Canavan et al. [23, 50]

$$\text{Turnover Efficiency} = \eta_{TOF} = \frac{(\text{Dynamic TOF}) - (\text{Average steady state TOF})}{(\text{Oscillation Frequency})} \quad (3)$$

$$\text{Effective TOF} = \eta_{TOF} \times \text{TOF}. \quad (4)$$

The weak oscillation frequency dependence of the TOF is also evident in the associated Arrhenius plot shown in **Figure 6C**, where only the 10 Hz oscillation frequency shows deviation from Arrhenius behavior. Zero apparent barrier for 10 Hz oscillation between 600 – 680 K suggests temperature independence of rate in this temperature range. This independence arises because the surface is saturated with NH_3* at +0.07 $|e^-|$/Ru atom for oscillation frequency 10 Hz as shown in **Figure 8D** which inhibits further N_2 activation and NH_x* hydrogenation to form additional NH_3* on the surface and therefore does not result in rate improvement with increasing temperature. Beyond 680 K, the adsorbed NH_3* can desorb from the surface resulting in vacant sites which would promote ammonia synthesis and therefore show a non-zero apparent barrier at higher temperatures. Zero apparent barrier is not observed for oscillation frequency > 10 Hz due to faster oscillation of surface charge to +0.04 |e-|/Ru atom which would promote ammonia desorption before the surface is saturated by NH_3* at +0.07 |e-|/Ru atom.

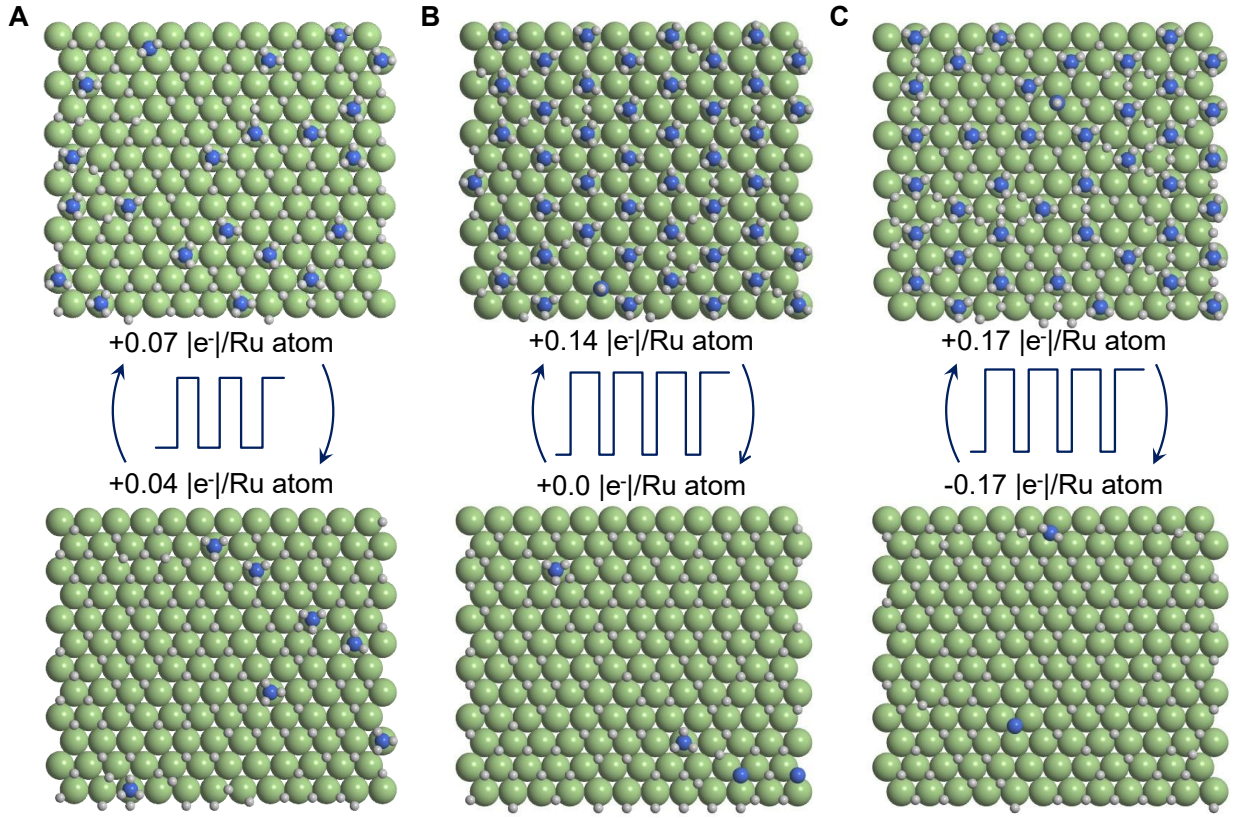

Figure 7. The ruthenium surfaces from kinetic Monte Carlo simulations under dynamic oscillation, with oscillation between **(A)** +0.04 $|e^-|$/Ru atom and +0.07 $|e^-|$/Ru atom using symmetric square wave oscillation function, **(B)** neutral and +0.14 $|e^-|$/Ru atom using asymmetric square wave oscillation function, and **(C)** -0.17 $|e^-|$/Ru atom and +0.17 $|e^-|$/Ru atom using asymmetric square wave oscillation function.

To improve the catalytic response of dynamic modulation of surface charge, we explore oscillation between neutral and +0.14 $|e^-|$/Ru, which are further away from the optimum charge using asymmetric square wave oscillation. A short time period (10^{-6} s) is used for neutral surface charge to enable the fast NH_3* desorption steps while avoiding N_2 activation at neutral surface charge and maintain effective step decoupling. An ideal catalytic turnover would involve N_2 activation and sequential NH_x hydrogenation steps to NH_3* at +0.14 $|e^-|$/Ru atom followed by oscillation to neutral charge for NH_3* desorption, as shown by the arrows in the reaction coordinate diagram in **Figure 6D**. However, the barriers for NH_3* dissociation is slightly lower than the NH_3* dissociation at neutral surface, making the preferred pathway sensitive to local surface configuration and lateral adsorbate

interactions captured within the kMC simulation. For example, the temporal surface coverage evolution plot in **Figure 8B** at 650 K and 10^3 oscillation frequency shows high NH_3* surface coverage at the end of +0.14 $|e^-|$/Ru period and at the onset of neutral charge, resulting in strong repulsion from neighboring ammonia molecules. This results in weaker NH_3* binding energy making NH_3* desorption more favorable over NH_3* dissociation and therefore results in ~0 ML surface coverage of NH_3* at the end of neutral and the start of +0.14 |e-|/Ru charge regime. In addition, increase in NH_3* surface coverage is accompanied by decrease in H* surface coverage, which is known through previous NH_3* and H* co-adsorption experimental studies. [46, 51]

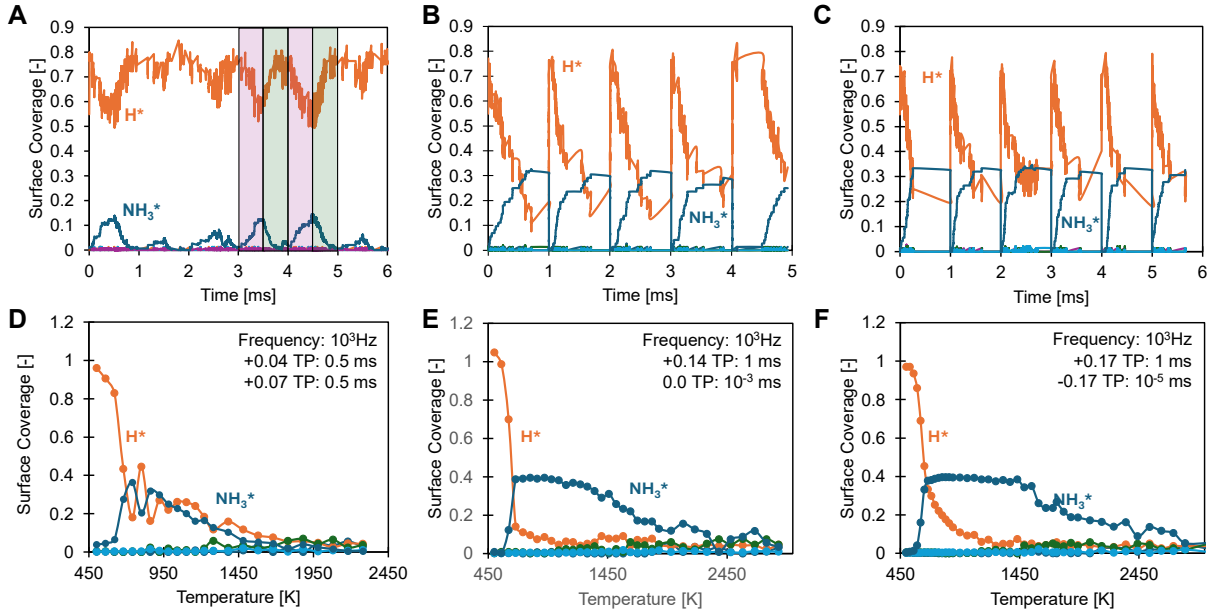

Figure 8. (A,B,C) The temporal evolution of surface coverage under dynamic oscillation of the surface charge density between +0.04 $|e^-|$/Ru atom and +0.07 $|e^-|$/Ru atom; neutral and +0.14 $|e^-|$/Ru atom; -0.17 $|e^-|$/Ru atom and +0.17 $|e^-|$/Ru atom, respectively. **(D,E,F)** The time-averaged average surface coverage under positive surface charge as a function of temperature.

To understand the influence of oscillation frequency on the TOF, the time period of the +0.14 $|e^-|$/Ru atom was varied between 10^{-1} s to 10^{-5} s while maintaining the neutral charge phase duration constant at 10^{-6} s. At low oscillation frequency, the plot of TOF against oscillation frequency shown in **Figure 6E** shows linear increase in the oscillation frequency up to ~10^3 Hz and plateaus at higher frequency. The TOF plot at frequencies <10^3 Hz lies below the parity line because the maximum turnover in a single oscillation cycle is limited by the sub-mono layer 1/3 ML saturation surface coverage of NH_3, implying that three surface Ru atoms are required to form one ammonia molecule in a single charge oscillation cycle. The maximum TOF attained for oscillation between neutral and +0.14 $|e^-|$/Ru is 270 $NH_3Ru^{-1}s^{-1}$ at ~10^3 Hz oscillation frequency and coincides with the oscillation frequency corresponding to maximum of effective TOF. This frequency is the resonance frequency (f_{res}), which is also the lowest frequency at which maximum surface sites are utilized for catalytic turnover.

The Arrhenius plot for oscillation between +0.14 $|e^-|$/Ru and neutral charge shown in **Figure 6F** reveals distinct kinetic regimes across 500 – 2500 K, with stronger oscillation frequency dependence of rate compared to the previous dynamic oscillation case involving charges close to the optimum. At temperatures < 560 K, the TOF is invariant with oscillation frequency between 10 – 10^5 Hz and temperature dependent with the kMC calculated apparent barrier equal to 120 kJ/mol. The contribution towards the apparent barrier comes

from the rate-limiting N_2 activation step at +0.14 |e-|/Ru atom ($X_{DRC,1}$ = 1; 35 kJ/mol), and hydrogen adsorption-desorption equilibrium ($X_{TDRC,2}$ = 0.7; 70 kJ/mol). At temperatures above 560 K, the apparent barrier for oscillation frequencies < 10^3 Hz drops from 120 kJ/mol to 0 kJ/mol as the surface becomes saturated with NH_3* at +0.14 |e^-|/Ru surface charge. This saturation inhibits N_2 activation via repulsive lateral interactions, preventing further NH_3* formation on the surface and eliminating temperature dependence of rate. As a result, the rate at the zero apparent barrier regime for all the oscillation frequencies is ~ (Saturation Surface Coverage) × (Oscillation Frequency). The onset temperature for zero apparent barrier increases with oscillation frequency as higher oscillation frequency requires faster NH_3* formation rates to achieve NH_3* surface saturation. Consequently, TOF becomes frequency-dependent but temperature-independent in this temperature regime.

For oscillation frequencies > 10^3 Hz, the surface is not saturated with NH_3* below 860 K as oscillation frequency is higher than the rate to reach NH_3* surface saturation. As a result, a non-zero apparent barrier of 50 kJ/mol is observed for frequencies higher than 10^4 Hz with N_2 activation step being the sole rate-limiting step. The thermodynamic degree of rate control for hydrogen adsorption desorption is close to zero due to low atomic hydrogen surface coverage at the operating temperature range, as shown in **Figure 8E**. For intermediate temperatures between 860 K – 1340 K and oscillation frequencies between 10 – 10^3 Hz, the apparent barrier increases gradually from 0 kJ/mol to ~250 kJ/mol. This arises from progressive NH_3* removal from the surface at 860 K, as repulsive lateral interactions under saturated NH_3* coverage weakens NH_3* binding strength resulting in lower barrier for NH_3* desorption and making NH_3* desorption kinetically feasible at 860 K. Repulsive lateral interactions decrease at these lower NH_3* coverages, which strengthens the binding energy of NH_3* and therefore increases the apparent activation barrier. In contrast, an apparent barrier of ~50 kJ/mol at 10^5 Hz oscillation frequency is observed which corresponds to the N_2 activation step as the surface never reaches NH_3* surface saturation between 860 – 1340 K. At temperatures greater than 1340 K, the apparent barrier drops from 250 kJ/mol to 32 kJ/mol for all oscillation frequencies, and the rate again becomes independent of the oscillation frequency. This drop is observed, because at these elevated temperatures ammonia desorption is no longer rate limiting and is faster than N_2 activation, which is limited by a low pre-exponential factor even at high temperatures.

To probe the maximum difference in the reaction coordinate for the charges under study, we examined oscillations between the extreme charge states of -0.17 |e^-|/Ru atom and +0.17 |e^-|/Ru atom using an asymmetric square wave oscillation function. To suppress N_2 activation at -0.17 |e^-|/Ru atom and thereby decouple the elementary steps, the time period for -0.17 |e^-|/Ru atom was restricted to 10^{-8} s corresponding to high NH_3* desorption rate. An ideal catalytic turnover would involve N_2 activation and sequential NH_x hydrogenation steps to NH_3* at +0.17 |e^-|/Ru atom followed by oscillation to -0.17 |e^-|/Ru for NH_3* desorption, as shown by the arrows in **Figure 6G**. The NH_3* desorption barrier is significantly lower than the NH_3* dissociation barrier at -0.17 |e^-|/Ru atom favoring NH_3* desorption over NH_3* dissociation under most surface configurations. This reaction coordinate is followed in the kMC simulations as indicated by the temporal evolution of surface coverages at 650 K and 10^3 Hz oscillation frequency shown in **Figure 8C**.

The plot of TOF as a function of oscillation frequency shown in **Figure 6H** exhibits similar trend to that for oscillation between +0.14 |e-|/Ru and neutral surface. The TOF increases linearly with oscillation frequency with a slope of 1/3 up to ~2 x 10^3 Hz and plateaus thereafter. The maximum TOF of ~620 $NH_3Ru^{-1}s^{-1}$ occurs at 2 x 10^3 Hz, with the peak shifted towards higher frequency compared to the previous case. The peak of the effective TOF aligns well with the maximum TOF resulting in the resonance frequency equal to ~2000 Hz.

The Arrhenius plot for dynamic oscillation between -0.17 and +0.17 |e^-|/Ru shown in **Figure 6I** suggests a similar progression of the kinetic regimes with increasing temperature similar to that observed in the previous dynamic oscillation case. At temperatures < 530 K, no rate enhancement with oscillation frequency is observed, and an apparent barrier of 120 kJ/mol arising from contributions from N_2 activation at the +0.17 |e^-|/Ru atom regime

and the hydrogen adsorption desorption equilibrium. At higher temperatures, NH_3* adsorbates accumulate and achieve saturation surface coverage leading to zero apparent barrier and frequency dependent rates for all the oscillation frequencies between 10 – 10^5 Hz. The onset temperature for zero apparent barrier increases with increasing frequency as higher oscillation frequency requires faster NH_3* formation rates to achieve NH_3* surface saturation. Further increase in temperature results in increasing rate for NH_3 desorption resulting in a gradual increase in the apparent barrier from 0 kJ/mol to ~230 kJ/mol. The TOF becomes frequency independent at temperatures > 1340 K. At temperatures > 1650K, the system transitions back to N_2 activation as the rate limiting step due to high NH_3* desorption rates and minimal NH_3* surface coverage as shown in the average surface coverage plot as a function of temperature in **Figure 8F**.

This study elucidates the distinct behaviors of catalytic ratchets enabled by dynamic surface charge modulation in programmable catalysis. Specifically, we observe both a leaky ratchet system (+0.04 and +0.07 $|e^-|$/Ru atom), a conditional efficient system (neutral and +0.14 $|e^-|$/Ru atom) and an efficient ratchet system (–0.17 and +0.17 $|e^-|$/Ru atom), with performance outcomes strongly dependent on the choice of charge states. While leaky ratchet system (+0.04 & +0.07 |e-|/Ru atom) did not provide significant rate enhancement over the rates at static +0.04 |e-|/Ru atom charge, the peak TOF was comparable to the ratchet system involving oscillation between neutral and +0.14 |e-|/Ru atom surface charge which showed significant influence of oscillation on TOF. Dynamic oscillations between extreme charge states (-0.17 & +0.17 |e-|/Ru atom) generated a three-fold rate enhancement over the leaky ratchet system. However, this enhancement remains modest primarily because of weak effect of surface charging on the N_2 activation barrier. The barrier decreases from 41 kJ/mol at neutral surface to 34 kJ/mol at +0.17 |e-|/Ru atom, limiting the overall rate gain achievable through dynamic oscillation. Therefore, further exploration of surface charging effects on alternative catalyst systems like nanoclusters, alloy surfaces or other transition metals through quantum mechanical calculations and experiments will be explored to further enhance the N_2 activation rate and make the programmable catalysis approach more viable for NH_3 synthesis.

Conclusions. The effect of forced dynamic surface charging of Ru surface on the NH_3 synthesis kinetics and the turnover frequency was highlighted using kinetic Monte Carlo simulations, guided by DFT calculations. DFT calculations by Ulrick et al. revealed that NH_x species exhibit stronger binding energy with more positive charge, with NH_3* showing the most pronounced sensitivity to surface charge density variation. The kMC simulations on statically-charged Ru surface showed that TOF increased with increasing static positive charge until +0.05 $|e^-|$/Ru atom, beyond which the rate declines due to excessively strong NH_3* binding energy that shifts the rate determining step from N_2 activation to NH_3* desorption. To overcome the limitations of static case, dynamic surface charge modulations were introduced to exploit faster N_2 activation rates at high positive surface charges. Three charge oscillation cases were explored: +0.04 & +0.07 $|e^-|$/Ru atom; neutral and +0.14 $|e^-|$/Ru atom; -0.17 and +0.17 $|e^-|$/Ru atom.

The different set of charges showed unique catalytic ratchets, and characteristically different kinetic regimes over the calculated range of oscillation frequencies and temperatures. Oscillation between +0.04 & +0.07 |e-|/Ru atom represented a ‘leaky’ catalytic system with small rate improvement over static rate at +0.04 |e-|/Ru atom till 10^3 Hz and no further rate enhancement at higher frequencies at 650 K. In addition, no discernible rate enhancement as a function of temperature was observed beyond 10^2 Hz. Oscillation between 0 & +0.14 |e-|/Ru atom yielded more ‘efficient’ ratchet with a peak TOF of 250 $NH_3Ru^{-1}s^{-1}$ at approximately 800 Hz at 650 K. The temperature-dependent kinetics revealed a shift in RDS from N_2 activation at low temperatures (<600 K) to NH_3* desorption at high temperatures (>1200 K), with a temperature-independent regime in between. The kinetic regimes observed are similar to the kinetic regimes reported by Jesse et al. in their theoretical investigation of programmable catalysis for a simple catalytic system $\left(A_{(g)} \rightarrow A^* \rightarrow B^* \rightarrow B_{(g)}\right)$. [22, 23] Finally, oscillation between –0.17 and +0.17 $|e^-|$/Ru atom, though yielding a threefold enhancement relative to the leaky system, showed limited improvement due to the weak sensitivity of N_2 activation to charge modulation on Ru surface.

Overall, dynamic charge oscillations enabled up to 20-fold enhancement in TOF compared to the neutral Ru surface. These findings highlight the potential of programmable catalysis to exceed static Sabatier limitations and motivate further exploration of charge-responsive surfaces, such as nanostructures or alternative metals, to enhance the viability of this approach for ammonia synthesis.

Acknowledgements. This work was supported as part of the Center for Programmable Energy Catalysis, an Energy Frontier Research Center funded by the U.S. Department of Energy, Office of Science, Basic Energy Sciences at the University of Minnesota under award #DE-SC0023464. Partial support for JRC was from the UMN West Central Research and Outreach Center Renewable Energy Program, made possible by State of Minnesota legislation for its Renewable Development Account. We acknowledge the Minnesota Supercomputing Institute (MSI) at the University of Minnesota for computational resources.

Keywords. Kinetic Monte Carlo, Programmable Catalysis, Ammonia Synthesis

Supporting Information. The Supporting Information is available free of charge at <link>:

Derivation of equations, kMC model parameters, adsorbate-adsorbate interaction model, transition state calculations, kMC methods

References

[1] S. Giddey, S. Badwal, C. Munnings and M. Dolan, "Ammonia as a renewable energy transportation media.," *ACS Sustainable Chemistry & Engineering,* vol. 5, no. 11, pp. 10231-10239, 2017.

[2] M. Palys, A. Allman and P. Daoutidis, "Exploring the benefits of modular renewable-powered ammonia production: A supply chain optimization study.," *Industrial & Engineering Chemistry Research,* vol. 58, no. 15, pp. 5898-5908, 2018.

[3] P. Barboun and J. Hicks, "Unconventional catalytic approaches to ammonia synthesis.," *Annual Review of Chemical and Biomolecular Engineering,* vol. 11, no. 1, pp. 503-521, 2020.

[4] A. Vojvodic, A. Medford, F. Studt, F. Abild-Pedersen, T. Khan, T. Bligaard and J. Nørskov, "Exploring the limits: A low-pressure, low-temperature Haber–Bosch process.," *Chemical Physics Letters,* vol. 598, pp. 108-112, 2014.

[5] C. Jacobsen, S. Dahl, B. Clausen, S. Bahn, A. Logadottir and J. Nørskov, "Catalyst design by interpolation in the periodic table: bimetallic ammonia synthesis catalysts.," *Journal of the American Chemical Society,* vol. 123, no. 34, pp. 8404-8405, 2001.

[6] G. Wittreich, S. Liu, P. Dauenhauer and D. Vlachos, "Catalytic resonance of ammonia synthesis by simulated dynamic ruthenium crystal strain.," *Science Advances,* vol. 8, no. 4, p. eabl6576, 2022.

[7] P. Stoltze, "Structure and surface chemistry of industrial ammonia synthesis catalysts," in *Ammonia: Catalysis and Manufacture*, Berlin, Heidelberg, Springer Berlin Heidelberg, 1995, pp. 17-102.

[8] J. Dumesic and A. Trevino, "Kinetic simulation of ammonia synthesis catalysis.," *Journal of Catalysis,* vol. 116, no. 1, pp. 119-129, 1989.

[9] S. Dahl, J. Sehested, C. Jacobsen, E. Törnqvist and I. Chorkendorff, "Surface science based microkinetic analysis of ammonia synthesis over ruthenium catalysts.," *Journal of Catalysis,* vol. 192, no. 2, pp. 391-399, 2000.

[10] J. M. J. Kammert, Y. Cheng, L. Daemen, S. Irle, V. Fung, J. Liu, K. Page, X. Ma, V. Phaneuf and J. Tong, "Nature of reactive hydrogen for ammonia synthesis over a Ru/C12A7 electride catalyst.," *Journal of the American Chemical Society,* vol. 142, no. 16, pp. 7655-7667, 2020.

[11] M. Hara, M. Kitano and H. Hosono, "Ru-loaded C12A7: e–electride as a catalyst for ammonia synthesis.," *ACS Catalysis,* vol. 7, no. 4, pp. 2313-2324, 2017.

[12] A. Baz, M. Lyons and A. Holewinski, "Dynamic electrocatalysis: Examining

resonant catalytic rate enhancement under oscillating electrochemical potential.," *Chem Catalysis,* vol. 2, no. 12, pp. 3497-3516, 2022.

[13] K. Hayashi, J. Griffin, K. Harper, Y. Kawamata and P. Baran, "Chemoselective (hetero) arene electroreduction enabled by rapid alternating polarity.," *Journal of the American Chemical Society,* vol. 144, no. 13, pp. 5762-5768, 2022.

[14] J. Timoshenko, A. Bergmann, C. Rettenmaier, A. Herzog, R. Arán-Ais, H. Jeon, F. Haase, U. Hejral, P. Grosse, S. Kühl and E. Davis, "Steering the structure and selectivity of CO2 electroreduction catalysts by potential pulses.," *Nature catalysis,* vol. 5, no. 4, pp. 259-267, 2022.

[15] C. Lim, M. Hülsey and N. Yan, "Non-faradaic promotion of ethylene hydrogenation under oscillating potentials.," *JACS Au,* vol. 1, no. 5, pp. 536-542, 2021.

[16] V. Vempatti, S. Wang, O. Abdelrahman, P. Dauenhauer and L. Grabow, "Catalytic Resonance of Methane Steam Reforming by Dynamically Applied Charges.," 2024.

[17] K. Bal, S. Huygh, A. Bogaerts and E. Neyts, "Effect of plasma-induced surface charging on catalytic processes: application to CO2 activation.," *Plasma Sources Science and Technology,* vol. 27, no. 2, p. 024001, 2018.

[18] A. Lele, Y. Xu and Y. Ju, "Modelling the effect of surface charging on plasma synthesis of ammonia using DFT.," *Physical Chemistry Chemical Physics,* vol. 26, no. 12, pp. 9453-9461, 2024.

[19] K. Oh, A. Walton, J. Chalmers, J. Hopkins, J. Canavan, T. Onn, S. Scott, C. Frisbie and P. Dauenhauer, "Alumina–Titania Nanolaminate Condensers for Hot Programmable Catalysis," *ACS Materials Letters,* vol. 6, pp. 3478-3486, 2024.

[20] T. Onn, S. Gathmann, S. Guo, S. Solanki, A. Walton, B. Page, G. Rojas, M. Neurock, L. Grabow, K. Mkhoyan and O. Abdelrahman, "Platinum graphene catalytic condenser for millisecond programmable metal surfaces.," *Journal of the Americal Chemical Society,* vol. 144, no. 48, pp. 22113-22127, 2022.

[21] T. Onn, K. Oh, D. Adrahtas, J. Soeherman, J. Hopkins, C. Frisbie and P. Dauenhauer, "Flexible and Extensive Platinum Ion Gel Condensers for Programmable Catalysis.," *ACS nano,* vol. 18, no. 1, pp. 983-995, 2023.

[22] J. Canavan and O. F. B. D. P. Abdelrahman, "Catalytic Resonance Theory: Experimental and Kinetic Interpretation of Programmable Catalysis," *ChemRxiv. [Preprint],* pp. https://doi.org/10.26434/chemrxiv-2025-32fdk, 2025.

[23] J. Canavan, J. Hopkins, B. Foley, O. Abdelrahman and P. Dauenhauer, "Catalytic Resonance Theory: Turnover Efficiency and the Resonance Frequency.," *ACS Catalysis,* vol. 15, no. 2, pp. 653-663, 2024.

[24] G. Kresse and J. Hafner, "Ab Initio Molecular Dynamics for Liquid Metals.," *Phys. Rev. B,* vol. 47, no. 1, p. 558–561, 1993.

[25] G. Kresse and J. Hafner, "Ab Initio Molecular-Dynamics Simulation of the Liquid-Metal-Amorphous-Semiconductor Transition in Germanium.," *Phys. Rev. B,* vol. 49, no. 20, pp. 14251-14269, 1994.

[26] G. Kresse and J. Furthmüller, "Efficient Iterative Schemes for Ab Initio Total-Energy Calculations Using a Plane-Wave Basis Set," *Phys. Rev. B,* vol. 54, no. 16, p. 11169–11186, 1996.

[27] G. Kresse and J. Furthmüller, "Efficiency of Ab-Initio Total Energy Calculations for Metals and Semiconductors Using a Plane-Wave Basis Set.," *Comput. Mater. Sci,* vol. 6, no. 1, pp. 15-50, 1996.

[28] J. P. Perdew, K. Burke and M. Ernzerhof, "Generalized Gradient Approximation Made Simple.," *Phys. Rev. Lett,* vol. 77, no. 18, p. 3865–3868, 1996.

[29] G. Kresse and D. Joubert, "From Ultrasoft Pseudopotentials to the Projector Augmented-Wave Method.," *Phys. Rev. B,* vol. 59, no. 3, p. 1758–1775, 1999.

[30] D. Gillespie, "A general method for numerically simulating the stochastic time evolution of coupled chemical reactions.," *Journal of computational physics,* vol. 22, no. 4, pp. 403-434, 1976.

[31] E. Hansen, Methodology for stochastic simulations of surface kinetics from first-principles., University of Virginia, 2001.

[32] E. Dybeck, C. Plaisance and M. Neurock, "Generalized temporal acceleration scheme for kinetic monte carlo simulations of surface catalytic processes by scaling the rates of fast reactions.," *Journal of chemical theory and computation,* vol. 13, no. 4, pp. 1525-1538, 2017.

[33] E. Shustorovich and H. Sellers, "The UBI-QEP method: a practical theoretical approach to understanding chemistry on transition metal surfaces.," *Surface science reports,* vol. 31, no. 1-3, pp. 1-119, 1998.

[34] E. Shustorovich, "Coverage effects under atomic chemisorption: Morse-potential modeling based on bond-order conservation.," *Surface Science,* vol. 163, no. 1, pp. L645-L654, 1985.

[35] T. Halgren, "Merck molecular force field. II. MMFF94 van der Waals and electrostatic parameters for intermolecular interactions.," *Journal of Computational Chemistry,* vol. 17, no. 5-6, pp. 520-552, 1996.

[36] H. Sellers and E. Shustorovich, "Intrinsic activation barriers and coadsorption effects for reactions on metal surfaces: unified formalism within the UBI-QEP approach.," *Surface science,* vol. 504, pp. 167-182, 2002.

[37] E. Shustorovich, "Bond making and breaking on transition-metal surfaces: theoretical projections based on bond-order conservation.," *Surface Science Letters,* vol. 176, no. 3, pp. L863-L872, 1986.

[38] S. Dahl, E. Törnqvist and I. Chorkendorff, "Dissociative adsorption of N2 on Ru (0001): a surface reaction totally dominated by steps.," *Journal of Catalysis,* vol. 192, no. 2, pp. 381-390, 2000.

[39] F. García-García, A. Guerrero-Ruiz and I. Rodríguez-Ramos, "Role of B5-type sites in Ru catalysts used for the NH3 decomposition reaction.," *Topics in catalysis,* vol. 52, pp. 758-764, 2009.

[40] Á. Logadóttir and J. Nørskov, "Ammonia synthesis over a Ru (0001) surface studied by density functional calculations.," *Journal of Catalysis,* vol. 220, no. 2, pp. 273-279, 2003.

[41] C. Jacobsen, S. Dahl, P. Hansen, E. Törnqvist, L. Jensen, H. Topsøe, D. Prip, P. Møenshaug and I. Chorkendorff, "Structure sensitivity of supported ruthenium catalysts for ammonia synthesis.," *Journal of Molecular Catalysis A: Chemical,* vol. 163, no. 1-2, pp. 19-26, 2000.

[42] A. Karim, V. Prasad, G. Mpourmpakis, W. Lonergan, A. Frenkel, J. Chen and D. Vlachos, "Correlating particle size and shape of supported Ru/γ-Al2O3 catalysts with NH3 decomposition activity.," *Journal of the American Chemical Society,* vol. 131, no. 34, pp. 12230-12239, 2009.

[43] I. Kurganskaya, N. Trofimov and A. Luttge, "A kinetic Monte Carlo approach to model Barite dissolution: the role of reactive site geometry.," *Minerals,* vol. 12, no. 5, p. 639, 2022.

[44] C. Benndorf and T. Madey, "Adsorption and orientation of NH3 on Ru (001).," *Surface science,* vol. 135, no. 1-3, pp. 164-183, 1983.

[45] H. Meskine, S. Matera, M. Scheffler, K. Reuter and H. Metiu, "Examination of the concept of degree of rate control by first-principles kinetic Monte Carlo simulations.," *Surface Science,* vol. 603, no. 10-12, pp. 1724-1730, 2009.

[46] S. Siporin and R. Davis, "Use of kinetic models to explore the role of base promoters on Ru/MgO ammonia synthesis catalysts.," *journal of Catalysis,* vol. 225, no. 2, pp. 359-368, 2004.

[47] B. McClaine, T. Becue, C. Lock and R. Davis, "Kinetic analysis of ammonia synthesis catalyzed by barium-promoted ruthenium supported on zeolite X.," *Journal of Molecular Catalysis A: Chemical,* vol. 163, no. 1-2, pp. 105-116, 2000.

[48] C. Fishel, R. Davis and J. Garces, "Ammonia synthesis catalyzed by ruthenium supported on basic zeolites.," *Journal of Catalysis,* vol. 163, no. 1, pp. 148-157, 1996.

[49] M. Murphy, S. Gathmann, R. Getman, L. Grabow, O. Abdelrahman and P. Dauenhauer, "Catalytic resonance theory: the catalytic mechanics of programmable ratchets.," *Chemical Science,* vol. 15, no. 34, pp. 13872-13888, 2024.

[50] M. Shetty, A. Walton, S. Gathmann, M. Ardagh, J. Gopeesingh, J. Resasco, T. Birol, Q. Zhang, M. Tsapatsis, D. Vlachos, P. Christopher, C. Frisbie, O. Abdelrahman and P. Dauenhauer, "The catalytic mechanics of dynamic surfaces: stimulating methods for promoting catalytic resonance," *ACS Catalysis,* vol. 10, no. 21, pp. 12666-12695, 2020.

[51] L. Danielson, M. Dresser, E. Donaldson and J. Dickinson, "Adsorption and desorption of ammonia, hydrogen, and nitrogen on ruthenium (0001).," *Surface Science,* vol. 71, no. 3, pp. 599-614, 1978.